Uniform Analytical Solution for Scattering by Circular PEC Apertures via Detour-Enhanced Extended BDW Theory

M. Altinel[a,b,*] and U. Yalçin[b]

[a]*Electronic Communication Technology Program, Mudanya University, Çağrışan Campus, 16940 Mudanya, Bursa, Türkiye*
[b]*Department of Electrical and Electronics Engineering, Bursa Uludag University, Görükle Campus, 16059 Nilüfer, Bursa, Türkiye*

Received: 26.10.2025 & Accepted: 20.04.2026

Doi: 10.12693/APhysPolA.149.134 *e-mail: altinelmust@gmail.com

We present a uniform analytical formulation for electromagnetic scattering by a circular aperture in an infinite perfectly electrically conducting plane. The formulation extends the boundary diffraction wave theory by incorporating both incident and reflected field contributions into a single analytical framework. A detour parameter combined with Fresnel uniformization is used to obtain a continuous edge-integral representation through the light–shadow transition. The resulting formulation reduces the aperture problem to a one-dimensional rim contribution and provides a compact analytical description of circular-aperture diffraction from a conducting screen over the considered angular range. Numerical evaluations based on the derived expressions illustrate the smooth behavior of the angular field, the symmetry associated with the conducting boundaries, and the edge-enhanced oscillatory features arising from the combined incident, reflected, and diffracted contributions. The main contribution of the study is a detour-enhanced uniform boundary diffraction wave formulation that provides a compact analytical representation of conductive circular-aperture diffraction and establishes a structured basis for future comparison with full-wave numerical and experimental benchmarks.

topics: electromagnetic scattering, boundary diffraction wave theory, Fresnel uniformization, circular perfectly electrically conducting (PEC) aperture

1. Introduction

The scattering of electromagnetic waves by apertures on perfectly electrically conducting (PEC) surfaces has long represented a cornerstone problem in classical wave theory, forming the basis of modern optics and electromagnetic modeling. Following Kirchhoff's pioneering formulation, the seminal works of Born and Wolf [1], Keller [2], and Miyamoto and Wolf [3] established the theoretical framework that evolved into the boundary diffraction wave (BDW) theory. This formulation, rooted in the Maggi–Rubinowicz concept, interprets the total field as the superposition of incident and edge-diffracted components — a conceptual advance that remains central to analytical diffraction modeling [4, 5].

Despite its theoretical elegance, the classical BDW theory exhibits non-uniform behavior near the light–shadow boundaries, producing unphysical discontinuities that limit its applicability, especially for curved apertures. Various uniformization strategies, including the use of asymptotic Fresnel integrals [6], paraxial diffraction expansions at the boundary [4], and analytical treatments bridging the Fresnel–Fraunhofer regimes [7, 8], have significantly improved the canonical diffraction modeling. However, a fully uniform analytical representation for circular PEC apertures has remained elusive. Recent theoretical and numerical studies have attempted to overcome this limitation through high-order Fresnel formulations [5, 9], hybrid analytic–numerical approaches [10], and sector-based aperture analyses [7]. Efficient computational techniques — such as non-uniform fast Fourier transform (FFT) implementations for Fresnel diffraction [5] and analytical–numerical coupling for curved PEC arcs [10] — have improved modeling accuracy but still rely on non-uniform field approximations. In parallel, analytical treatments of specialized geometries, including pseudo-nondiffracting Bessel beams [11] and resistive circular holes [12], have broadened the theoretical landscape yet failed to fully resolve the PEC uniformization problem.

In the broader electromagnetic context, diffraction by circular apertures continues to play a key role in high-frequency and computational electromagnetics [9, 13, 14]. For example, Lovat et al. [13] analyzed magnetic field penetration through circular PEC plates, while Serdyuk [14] examined diffraction through finite-thickness conductors. Similarly, Wang et al. [15] demonstrated ultra-low-threshold lasing through metallic circular apertures, and Zhou et al. [16] investigated near-field coupling effects in PEC screens — both highlighting the continuing relevance of analytical modeling to photonics and antenna engineering. In this context, several extensions of BDW theory have been proposed. Umul [5] and Yalçın [17] introduced the uniform boundary diffraction wave theory, while Altınel and Yalçın [18, 19] extended it to perfect magnetic conductor (PMC) and opaque surfaces within the extended BDW (EBDW) framework. Additional refinements addressed boundary impedance effects [20], composite mixed-boundary problems [10], and aperture-specific Fresnel diffraction behaviors [21, 22]. Nevertheless, a comprehensive and truly uniform analytical solution for circular PEC apertures, integrating both incident and reflected field components, has not yet been realized.

Beyond the theoretical challenge, modern applications in metasurface design and high-resolution imaging impose stringent requirements of accuracy and efficiency. Studies such as Gao et al. [23] and Aime et al. [24] emphasize the need for diffraction models capable of resolving subwavelength or starshade-scale features with minimal computational cost. These demands motivate the development of new analytical formulations that combine physical rigor with numerical efficiency.

In this work, we develop a detour-enhanced uniform analytical formulation for electromagnetic scattering by a circular aperture in an infinite PEC plane. Building upon the vector-potential-based BDW formulation and its detour-enhanced extensions [4, 19], the proposed method incorporates both incident and reflected PEC contributions within a single edge-integral kernel. By combining the detour parameter with asymptotic Fresnel uniformization, the formulation provides a continuous one-dimensional representation through the light–shadow transition for the considered observation directions. Numerical evaluations for different aperture radii and observation distances illustrate angular continuity, symmetry, and PEC-related edge-enhanced oscillatory behavior predicted by the analytical model. The contribution of this work is therefore a compact and physically interpretable uniform BDW-based framework for conductive circular apertures, rather than a replacement for full-wave numerical solvers.

By addressing both theoretical limitations and a computational challenge, the present study provides a consistent analytical framework that can support future developments in computational electromagnetics, metasurface design, and wave-based engineering.

2. Theory and analytical formulation

The diffraction of an electromagnetic wave by a circular perfectly conducting (PEC) aperture can be rigorously derived within the boundary-diffraction-wave (BDW) framework based on the classical Helmholtz–Kirchhoff integral [1]. In the present formulation, a time harmonic-plane-wave excitation is assumed, and the total scalar field $U(P)$ is evaluated at an observation point P enclosed by a surface S. Here, $U(P)$ is used as a representative scalar component of the electromagnetic field. For clarity, the numerical evaluations are interpreted in terms of the linearly polarized electric-field component associated with the incident wave. The use of a scalar component does not imply that the PEC boundary conditions are neglected; rather, the PEC response is introduced through the incident and reflected field contributions in the boundary kernel. On the perfectly conducting plane, the tangential electric field satisfies the PEC condition, while the reflected contribution includes the corresponding phase reversal. Therefore, the scalar BDW formulation employed here should be understood as a component-level reduction of the electromagnetic aperture problem, not as a full vector modal solution. The field is expressed as

$$U(P) = \oiint_S \mathrm{d}S \;\; \boldsymbol{V}(Q,P) \cdot \boldsymbol{n}, \tag{1}$$

where Q is a variable source point on the surface S, $\boldsymbol{n}$ is the inward unit normal on S, and $\boldsymbol{V}(Q,P)$ is the vector kernel that ensures $U(P)$ satisfies the homogeneous Helmholtz equation [1]. Equation (1) forms the mathematical foundation of the theory of scalar diffraction and constitutes the starting point for the BDW approach originally developed by Miyamoto and Wolf [3].

Applying Stokes' theorem allows the total field to be separated into two physically distinct components, namely the geometrical optics (GO) field and the boundary-diffraction field [2, 3],

$$U(P) = U_B(P) + U_{\mathrm{GO}}(P). \tag{2}$$

Here, $U_{\mathrm{GO}}(P)$ represents the direct transmission predicted by geometrical optics, whereas $U_B(P)$ corresponds to the diffracted contribution generated at the aperture rim. This decomposition is crucial because it isolates the edge effects responsible for diffraction from the smooth propagation that follows geometrical optics.

The diffracted contribution $U_B(P)$ can be formulated as a contour integral over the aperture rim $\mathit{\Gamma}$ [3–5]

$$U_B(P) = \int_{\mathit{\Gamma}} \mathrm{d}l \;\; \boldsymbol{W}(Q,P) \cdot \boldsymbol{l}. \tag{3}$$

In this expression, $\mathit{\Gamma}$ denotes the circular boundary of the aperture, $\boldsymbol{l}$ is the unit tangent vector along the contour, and $\boldsymbol{W}(Q,P)$ is the BDW kernel. This compact integral form establishes a direct link

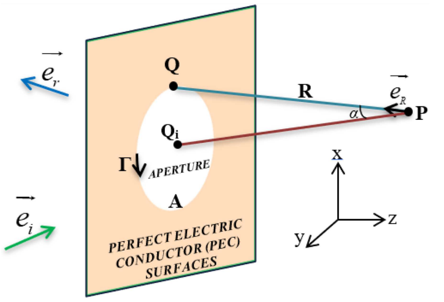

Fig. 1. Geometrical configuration showing the incident, reflected, and observation directions represented by the unit vectors $\boldsymbol{e}_i$, $\boldsymbol{e}_r$, and $\boldsymbol{e}_R$, respectively, as used in (11).

between the field at the observation point and the local field variations along the boundary. The explicit form of the BDW kernel is written as [3]

$$\boldsymbol{W}(Q,P) = \frac{\mathrm{e}^{-\mathrm{i}kR}}{R}\frac{\Big(\boldsymbol{e}_R\times\nabla_Q - \mathrm{i}k+\boldsymbol{e}_R\cdot\nabla_Q\Big)U(Q)}{4\pi}, \tag{4}$$

where $k = 2\pi/\lambda$ is the wavenumber associated with wavelength λ, $\boldsymbol{R} = \| \boldsymbol{r} - \boldsymbol{r'} \|$ is the distance between the observation point $P(\boldsymbol{r})$ and the boundary point $Q(\boldsymbol{r'})$, and $\boldsymbol{e}_R = (\boldsymbol{r} - \boldsymbol{r'})/R$ is the unit vector directed from Q to P. The operator ∇_Q acts on the boundary coordinates, and the exponential term accounts for the phase delay due to propagation. The three terms inside the brackets in (4) describe, respectively, the vector circulation, phase shift, and projection effects, which collectively define diffraction from the edge.

To maintain consistency with geometrical optics, the GO term is expressed as the limit of infinitesimal contour contributions [2]

$$U_{\mathrm{GO}}(P) = \sum_i \lim_{\sigma_i\to 0}\int_{\Gamma_i} \mathrm{d}l \;\; \boldsymbol{W}(Q_i,P)\cdot\boldsymbol{l}. \tag{5}$$

This form ensures a continuous transition between illuminated and shadowed regions as the observation point crosses the geometrical boundary.

In the following section, we apply the analytical formulation, rigorously derived from Maxwell's equations, to the scattering problem of a circular aperture on an infinite PEC plane.

To specify the boundary conditions for the aperture, in the case of plane-wave illumination, the reference incident and reflected fields are expressed, respectively, as [3–5]

$$U_i(P) = u_i\,\mathrm{e}^{-\mathrm{i}kr\cos(\theta)}, \tag{6}$$

and

$$U_r(P) = -u_i\,\mathrm{e}^{\,\mathrm{i}kr\cos(\theta)}, \tag{7}$$

where u_i is the complex amplitude of the incident wave, and $(r,\,\theta,\,\phi)$ are the spherical coordinates of the observation point P measured from the aperture axis (the z-axis). The reflected term has a negative sign, indicating phase reversal produced by the PEC boundary. This sign convention corresponds to the selected tangential electric-field component under assumed linear polarization and is consistent with the PEC condition on the conducting surface. These two plane waves form the reference fields required in the kernel evaluation.

The scalar distance between the observation point and a point on the circular aperture rim is first written in its general azimuth-dependent form. For the observation point $P(r,\theta,\phi)$ and the rim point $Q(a,\phi')$ located on the plane $z' = 0$, the general rim-to-observer distance is

$$R_e = |\boldsymbol{R}| = \sqrt{(x-x')^2 + (y-y')^2 + (z-z')^2}. \tag{8}$$

This expression preserves the full dependence on the rim azimuth ϕ' and is the distance used in the original contour-integral representation. In the reduced notation used after evaluating the stationary phase, R_e denotes the effective detour distance evaluated at the stationary rim direction. For the stationary direction $\phi' = \phi$, one obtains $\cos(\phi - \phi') = 1$, and therefore

$$R_e = \sqrt{r^2 + a^2 - 2\,ar\sin(\theta)}. \tag{9}$$

Thus, R_e should not be interpreted as the general rim-to-observer distance inside the original contour integral; it is the stationary-point effective distance used after asymptotic reduction. This clarification removes the apparent inconsistency between the definition of the distance and the dependence $\cos(\phi - \phi')$ appearing later in (15).

The spatial derivative of the boundary field in (4) is governed by the directions of incidence and reflection, giving

$$\nabla_Q U(Q) = -\mathrm{i}k\; u_i\big(\boldsymbol{e}_i - \boldsymbol{e}_r\big), \tag{10}$$

where $\boldsymbol{e}_i$ and $\boldsymbol{e}_r$ are unit vectors in the incident and reflected directions, respectively. Substituting (10) into (4) yields the explicit BDW kernel, which contains both directional and amplitude information [3, 5, 9]. This substitution connects the field derivative at the aperture boundary directly to the known incident and reflected field directions, linking geometry with the physical boundary conditions.

After substituting (10) into (4), the explicit boundary-diffraction-wave kernel is obtained as

$$\boldsymbol{W}(Q,P) = \frac{u_i}{4\pi}\frac{\mathrm{e}^{-\mathrm{i}kR}}{R}\left(\frac{\boldsymbol{e}_R\times\boldsymbol{e}_i}{1+\boldsymbol{e}_R\cdot\boldsymbol{e}_i} - \frac{\boldsymbol{e}_R\times\boldsymbol{e}_r}{1+\boldsymbol{e}_R\cdot\boldsymbol{e}_r}\right). \tag{11}$$

explicitly separates the incident and reflected contributions through their directional dependence, ensuring the kernel satisfies the boundary conditions on the PEC plane.

The configuration, illustrated in Fig. 1, provides a clear physical interpretation of the BDW kernel in (11). The unit vectors $\boldsymbol{e}_i$ and $\boldsymbol{e}_r$ represent the incident and reflected field directions relative to the PEC surface, respectively, while $\boldsymbol{e}_R$ connects the boundary point Q to the observation point P. The vector $\boldsymbol{R}$ and the associated angle α describe the propagation path and the orientation between the reflected ray and the observer. These geometric relations explain the presence of cross and dot products in (11), which together account for the amplitude and directional dependence of the diffracted field generated at the aperture rim.

The vector relationships used in (11) are obtained from simple geometry [3, 5, 9]. The unit vector $\boldsymbol{e}_R$, which connects the boundary and observation points, is written as

$$\boldsymbol{e}_R = \frac{a\,\boldsymbol{e}_\rho' - r\,\boldsymbol{e}_r}{R}, \tag{12}$$

where $\boldsymbol{e}_{\rho'} = \cos(\phi')\,\boldsymbol{e}_x + \sin(\phi')\,\boldsymbol{e}_y$ is the radial unit vector in the aperture plane at the boundary point Q, and $\boldsymbol{e}_x\boldsymbol{e}_y\boldsymbol{e}_z$ denote the Cartesian basis vectors. The observation-direction unit vector $\boldsymbol{e}_r$ is given by

$$\boldsymbol{e}_r = \sin(\theta)\cos(\phi)\boldsymbol{e}_x + \sin(\theta)\sin(\phi)\boldsymbol{e}_y + \cos(\theta)\boldsymbol{e}_z, \tag{13}$$

where θ and ϕ are the polar and azimuthal coordinates of the observation point P, respectively. These relations define the geometric link between the boundary and the observer, ensuring that all directional quantities in (11) are explicitly defined and physically interpretable.

The differential element of the rim contour, required in the integration of (3), is expressed as [3, 5, 18]

$$\mathrm{d}\boldsymbol{l} = a\,\sin(\theta)\;\mathrm{d}\phi'\,\boldsymbol{e}_\phi, \tag{14}$$

where $\boldsymbol{e}_\phi$ denotes the azimuthal unit vector used in the observation-coordinate representation of the BDW kernel. The same local rim element can equivalently be written in the intrinsic rim basis as $\mathrm{d}\boldsymbol{l}_0 = a\,d\,\phi'\,\boldsymbol{e}_{\phi'}$, where $\boldsymbol{e}_{\phi'}$ is the local unit vector tangent to the circular aperture rim. Therefore, the factor $\sin(\theta)$ in (14) should be interpreted as a projection factor arising from the observation-coordinate representation of the kernel, rather than as a modification of the physical contour length. This clarification ensures consistency between the local rim basis and the observation-coordinate basis.

Figure 2 illustrates the local geometry of the circular aperture on the PEC surface and shows how the differential contour element $\mathrm{d}\boldsymbol{l}$ is oriented along the rim. The azimuthal unit vector $\boldsymbol{e}_\phi$ defines the tangential direction of integration, while the radial distance a and the polar angle θ determine the projection of the rim onto the plane x–y. This geometric relationship clarifies the physical meaning of (14), which connects the mathematical contour element with the actual edge of the aperture, where the diffracted field originates.

In summary, the sequence of (1)–(14) establishes a complete analytical description of the boundary-diffraction-wave formulation for a circular PEC aperture. This classical structure, first introduced in [3] and later extended by [5, 9, 11, 19], provides the groundwork for the uniform analytical solution presented in the next section. The field $U_B(P)$ is defined as a contour integral whose kernel $\boldsymbol{W}(Q,P)$ is explicitly expressed in terms of known geometric quantities and parameters of the incident wave. All variables necessary for subsequent numerical or asymptotic evaluations have now been established. In the next section, these relations are used to derive a closed-form uniform analytical solution that remains valid in both illuminated and shadow regions, thereby eliminating the discontinuities inherent in purely geometrical optics descriptions.

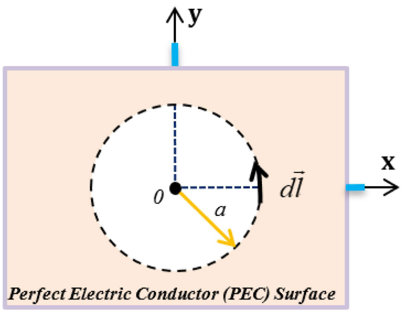

Fig. 2. Geometry of the circular PEC aperture and the projected differential contour element defined in (14).

3. Uniform analytical solution

The analytical formulation developed in Sect. 2 provides the complete boundary-diffraction-wave (BDW) representation of the field scattered by a circular perfectly electrically conducting (PEC) aperture. However, as identified in the classical works of Miyamoto and Wolf [3], conventional BDW theory exhibits non-uniform behavior near the geometrical shadow boundary. In this region, the field predicted by geometrical optics (GO) abruptly transitions into the diffracted component, producing amplitude discontinuities that lack physical realism. To overcome this long-standing limitation, the present section introduces a rigorously derived uniform analytical formulation that combines the detour concept and Fresnel's asymptotic uniformization. This approach yields a closed-form, continuous solution valid for all observation angles, in both illuminated and shadow regions.

Starting from the edge-integral representation, the boundary field for a circular PEC aperture is expressed as

$$U_B(P) = \frac{u_i\,a\sin(\theta)}{4\pi}\int_0^{2\pi}\mathrm{d}\phi'\,\Big[r\sin(\theta)\cos(\phi-\phi')-a\Big] \times \left(\frac{1}{R-r\cos(\theta)} + \frac{1}{R+r\cos(\theta)}\right)\frac{\mathrm{e}^{-\,\mathrm{i}kr}}{R}, \tag{15}$$

In (15), u_i is the complex amplitude of the incident wave, r and θ denote the radial distance and polar angle of the observation point P, respectively, while ϕ and ϕ' represent the azimuthal coordinates of the observation and rim points, respectively. The variables a and R correspond to the aperture radius and the distance between the boundary point and the observation point, respectively. This integral form establishes a relationship between the diffracted field and the aperture edge geometry.

To derive a compact analytical expression, the integral in (15) is evaluated using the stationary phase method, which retains the dominant contributions from the aperture rim. The stationary-phase reduction used in this step is an asymptotic approximation. Its accuracy improves when the effective phase parameter is sufficiently large, particularly for configurations in which kR_e and the aperture-related phase variation along the rim are not small. Therefore, the expression we are heading forward should be interpreted as the leading asymptotic edge contribution extracted from (15), rather than as an exact evaluation of the full contour integral. The numerical cases including $a = \lambda$ and $r = 3\lambda$ are retained as examples of lower-bound transition in the considered parameter set. They are used to examine the continuity and qualitative angular behavior of the uniformized formulation near the lower end of the considered aperture-size and observation-distance range, rather than to claim strict asymptotic accuracy in the far field or independent benchmark-level validation. With these asymptotic considerations, the stationary-phase evaluation gives

$$U_B(P) \approx \frac{u_i}{2\sqrt{2\pi}}\sqrt{\frac{a\sin(\theta)}{r}}\,\big(r\sin(\theta)-a\big) \times \left[\frac{1}{R_e - r\cos(\theta)} + \frac{1}{R_e + r\cos(\theta)}\right]\frac{\mathrm{e}^{-\mathrm{i}\,(kR_e+\pi/4)}}{\sqrt{kR_e}}. \tag{16}$$

Here, R_e represents the effective optical distance along the detour path connecting the aperture rim and the observation point. Equation (16) establishes the asymptotic basis for the uniform solution, maintaining the physical features of the BDW kernel but requiring an additional transformation to ensure amplitude continuity at the light–shadow interface. However, this representation alone remains non-uniform and fails to capture the smooth phase evolution near the geometrical boundary, thereby motivating the introduction of the detour parameter in the subsequent formulation.

At this stage, a detour parameter (denoted as Δ) is introduced to describe the optical path difference between the geometrical and diffracted rays. This parameter enables the smooth transition between illuminated and shadowed domains. To implement this mathematically, the field is reformulated using the Fresnel transition function $\hat{F}(\xi_i)$, defined as

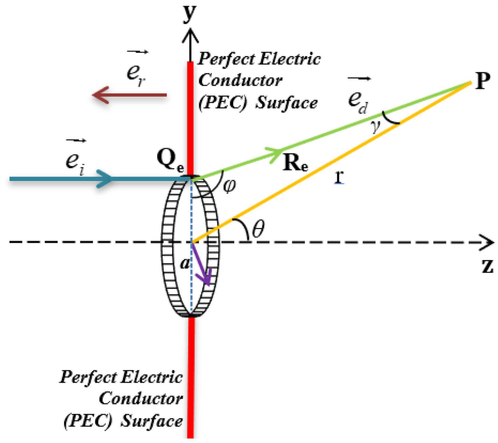

Fig. 3. Diffraction geometry of an incident field through a circular aperture on a perfectly electrically conducting (PEC) plane.

$$\hat{F}\,(\xi_i) = \frac{\mathrm{e}^{-\mathrm{i}\,(\xi_i^2+\pi/4)}}{2\sqrt{\pi}\,\xi_i}, \tag{17}$$

where the argument ξ_i is a dimensionless Fresnel variable controlling the phase detour, given by

$$\xi_i = -\sqrt{\psi_i - \psi_d} = -\sqrt{k\big(R_e - r\cos(\theta)\big)}. \tag{18}$$

The square of this variable satisfies

$$\xi_i^2 = kR_e - kr\,\cos(\theta) = kR_e - kz. \tag{19}$$

In these relations, $k = 2\pi/\lambda$ is the wavenumber, ψ_i and ψ_d denote the phase functions of the incident and detoured optical paths, respectively, and $z = r\cos(\theta)$ is the axial projection of the observation point. The Fresnel function $\hat{F}(\xi_i)$ ensures both analytical and physical continuity of the field amplitude and phase across the shadow boundary, resolving the non-physical discontinuity inherent in the original BDW model. This asymptotic uniformization concept was first generalized by Borghi [4] and later refined by Ganci [6] for extended aperture geometries.

The configuration in Fig. 3 illustrates the physical basis of the detour-enhanced diffraction process. An incident wave $\boldsymbol{e}_i$ impinges upon the PEC surface and generates a reflected component $\boldsymbol{e}_r$; both fields interact at the circular rim Q_e of radius a. From this rim, the diffracted wave $\boldsymbol{e}_d$ emerges and propagates toward the observation point $P(r, \theta, \phi)$ along the detour path of geometrical length $\boldsymbol{R}_e$. The angle γ describes the inclination between the detour direction and the observation axis, governing the transition between the illuminated and shadow regions.

This geometrical interpretation clarifies the analytical formulation introduced in (17)–(19), i.e., the detour parameter Δ defines the optical path difference between the direct and diffracted rays, ensuring that both the amplitude and phase of the total field remain continuous.

Consequently, the geometry allows for a visual understanding of how the incident and reflected fields at a PEC boundary jointly contribute to a uniform diffracted field, free from discontinuities across the light–shadow boundary. As illustrated in Fig. 3, the detour path of geometrical length $\boldsymbol{R}_e$ quantifies the accumulated phase of the diffracted ray relative to the direct propagation, while the detour parameter Δ measures the additional phase delay governing the transition between the illuminated and shadow regions.

With the Fresnel variable established, the uniform field can now be separated into its incident and reflected boundary contributions. Substituting (17) into (18) gives the incident-side boundary field as

$$U_{B_i}(P) = -\frac{u_i}{\sqrt{2}}\sqrt{\frac{a\sin(\theta)}{r}}\,(r\sin(\theta)-a) \times \frac{\mathrm{e}^{-\mathrm{i}kr\cos(\theta)}}{\sqrt{R_e\,(R_e - r\cos(\theta))}}\,\hat{F}\,(\xi_i)\,, \tag{20}$$

The function $\hat{F}(\xi_i)$ can be equivalently written in its canonical integral form [5] as

$$\hat{F}\,(\xi_i) = \frac{\mathrm{e}^{\,\mathrm{i}\pi/4}}{\sqrt{\pi}}\int_{\xi_i}^{\infty}\mathrm{d}t\ \ \mathrm{e}^{-\mathrm{i}t^2}, \tag{21}$$

This integral representation directly links the detour phase to the spatial frequency response of the aperture, allowing a unified description of diffraction and reflection. To fully represent the behavior of the PEC surface, a sign function $\operatorname{sgn}(\xi)$ is introduced [20] to distinguish the propagation direction of the field.

The incident and reflected boundary contributions thus become, respectively,

$$U_{B_i}(P) = -\frac{u_i}{\sqrt{2}}\sqrt{\frac{a\sin(\theta)}{r}}\,(r\sin(\theta)-a) \times \frac{\mathrm{e}^{-\mathrm{i}kr\cos(\theta)}}{\sqrt{R_e\,(R_e - r\cos(\theta))}}\,\hat{F}\,(|\xi_i|)\ \operatorname{sgn}(\xi_i)\,, \tag{22}$$

and

$$U_{B_r}(P) = -\frac{u_i}{\sqrt{2}}\sqrt{\frac{a\sin(\theta)}{r}}\,(r\sin(\theta)-a) \times \frac{\mathrm{e}^{-\mathrm{i}kr\cos(\theta)}}{\sqrt{R_e\,(R_e + r\cos(\theta))}}\,\hat{F}\,(|\xi_r|)\ \operatorname{sgn}(\xi_r)\,, \tag{23}$$

Here, ξ_r is the Fresnel variable corresponding to the reflected ray, which obeys a similar phase relation to (18), but with the opposite propagation direction. These expressions reveal the symmetry of PEC diffraction; both incident and reflected rays contribute to the boundary field, creating the physically consistent dual-wave behavior observed in PEC aperture scattering [13, 14].

The total boundary-diffraction field is obtained by superposing the incident and reflected contributions

$$U_B(P) = U_{B_i}(P) + U_{B_r}(P), \tag{24}$$

which yields,

$$U_B\,(P) = -\frac{u_i}{\sqrt{2}}\sqrt{\frac{a\sin(\theta)}{rR_e}}\big(r\sin(\theta){-}a\big)\ \left[\frac{\mathrm{e}^{-\mathrm{i}kr}}{\sqrt{R_e - z}}\,\hat{F}\,(|\xi_i|)\ \operatorname{sgn}(\xi_i) + \frac{\mathrm{e}^{\,\mathrm{i}kr}}{\sqrt{R_e + z}}\,\hat{F}\,(|\xi_r|)\ \operatorname{sgn}(\xi_r)\right]. \tag{25}$$

In (25), $\hat{F}(|\xi|)$ represents the Fresnel amplitude function derived from $\hat{F}(\xi)$. The presence of conjugate exponential terms $\mathrm{e}^{\pm\,\mathrm{i}kz}$ ensures the correct phase matching between the forward and backward propagating components. The resulting field exhibits continuous amplitude and phase across all angular domains, confirming the uniform validity of the detour-enhanced BDW formulation [9].

Finally, the total scattered field, including the geometrical-optics component $u_i\,\mathrm{e}^{-\mathrm{i}kz}$, can be expressed as

$$U_{\mathrm{ts}}(P) = U_{B_s}(P) = U_{B_i}(P) + U_{B_d}(P) + U_{B_r}, \tag{26}$$

which can be rearranged as

$$U_{B_s}(P) = u_i\,\mathrm{e}^{-\mathrm{i}kz}\,u(-\xi_i) - \frac{u_i}{\sqrt{2}}\sqrt{\frac{a\sin(\theta)}{rR_e}}\big(r\sin(\theta){-}a\big)\ \left[\frac{\mathrm{e}^{-\mathrm{i}kr}\,\hat{F}\,(|\xi_i|)\ \operatorname{sgn}(\xi_i)}{\sqrt{R_e{-}z}} + \frac{\mathrm{e}^{\,\mathrm{i}kr}\,\hat{F}\,(|\xi_r|)\ \operatorname{sgn}(\xi_r)}{\sqrt{R_e{+}z}}\right], \tag{27}$$

Here, $u(-\xi_i)$ is the unit step function identifying the illuminated region, while $U_{B_d}(P)$ represents the diffracted contribution. This diffracted term corresponds to the uniform boundary component defined earlier in (25), which ensures the continuous transition between the geometrical and diffracted fields.

Equation (27) constitutes the final uniform analytical solution for electromagnetic scattering from a circular PEC aperture. It rigorously integrates the incident, reflected, and diffracted components into a single continuous representation that remains valid in both near-field and far-field regimes.

Physically, this unified form shows how the detour parameter Δ governs the smooth transition between geometrical and diffracted contributions, ensuring a continuous field representation across the shadow boundary. The formulation also reproduces symmetric angular behavior and edge-enhanced oscillatory features associated with the reflective PEC boundary. These features are interpreted here as interference-related edge effects within the present analytical model, rather than as independently proven resonant modes [18, 19].

Mathematically, the combination of Fresnel uniformization and detour-enhanced edge integration establishes a continuous analytical bridge between the geometrical-optics limit and the diffracted field representation. The uniform analytical expressions established above form the basis of the numerical evaluations and comparative discussions presented in the next section.

4. Results and discussion

All numerical evaluations were performed using MATLAB R2023a on a standard workstation (Intel i7, 16 GB RAM). Angular profiles were computed with a resolution of 0.5°. The aperture radii ($a = \lambda$, 2λ, 3λ) and observation distances ($r = 3\lambda$, 6λ, 9λ) were selected to cover representative transition near-field and moderate far-field configurations within the analytical model. The scripts used to generate the figures are available upon request. The numerical results presented in this section are computed directly from the analytical expressions in (22)–(25). Therefore, they are used to examine the continuity, angular behavior, and parametric response of the proposed formulation and do not serve as independent full-wave simulations. Unless otherwise stated, fields are normalized to the peak magnitude of the total field at $\theta = 0°$.

In this section, the analytical framework developed in the previous sections is evaluated through numerical calculations based on the derived expressions. The main objective is to examine the continuity, angular behavior, and parameter dependence of the proposed detour-enhanced extended BDW formulation for circular PEC apertures. The results are discussed with reference to conventional BDW-based descriptions and related analytical models reported in the literature [13, 14, 18, 24]. The theoretical results predict distinct field behavior in the illuminated, shadow, and transition regions, with the transition region being particularly sensitive to the adopted uniformization scheme. Classical BDW theory is known to produce unphysical discontinuities at the shadow boundary [3], whereas the present formulation provides a continuous analytical field representation over the considered angular range.

Numerical evaluations were performed for a range of aperture radii and observation distances, with parameters selected to highlight the differences between PEC and opaque-surface representations and to examine PEC-related edge-enhanced oscillatory field behavior. The comparison is intended to show how the inclusion of the reflected contribution modifies the angular field structure within the BDW framework. No claim of independent full-wave benchmark validation is made in the present study; however, the results demonstrate the continuity and computational compactness of the proposed analytical representation.

To clarify the relation of the present formulation to established approaches, it is useful to distinguish between high-frequency asymptotic methods, small-aperture theories, modal formulations, and full-wave numerical solvers. GTD, UTD, and PTD-type approaches[†1] provide powerful ray- or current-based descriptions of diffraction from canonical edges and conducting structures, but they generally rely on local diffraction coefficients, ray tracing, or equivalent edge currents rather than on a detour-uniformized BDW rim integral for the complete circular aperture [2, 25]. Bethe-type aperture theory is especially effective in the subwavelength limit, where a small hole can be represented through equivalent electric and magnetic dipole moments; however, it is not intended to describe the full angular transition behavior of finite circular PEC apertures over the parameter range considered here [26]. Modal/eigenfunction-based circular-aperture formulations, including rigorous finite-thickness PEC-screen treatments, can provide detailed electromagnetic descriptions, but they require geometry-specific expansions or numerical implementation and are less compact than the present one-dimensional edge representation [27]. Full-wave solvers, e.g., MoM, FEM, and FDTD[†2], are suitable for independent benchmark validation and detailed field or current distributions, but require discretization, meshing, and numerical convergence control [28, 29]. The present formulation is therefore complementary to these methods. It does not replace full-wave benchmark solvers, but provides a compact, physically interpretable, and uniform BDW-based analytical framework in which the PEC-related incident and reflected contributions are incorporated directly into the

[†1] GTD — geometrical theory of diffraction; UTD — uniform theory of diffraction; PTD — physical theory of diffraction.

[†2] MoM — method of moments; FEM — finite element method; FDTD — finite-difference time-domain.

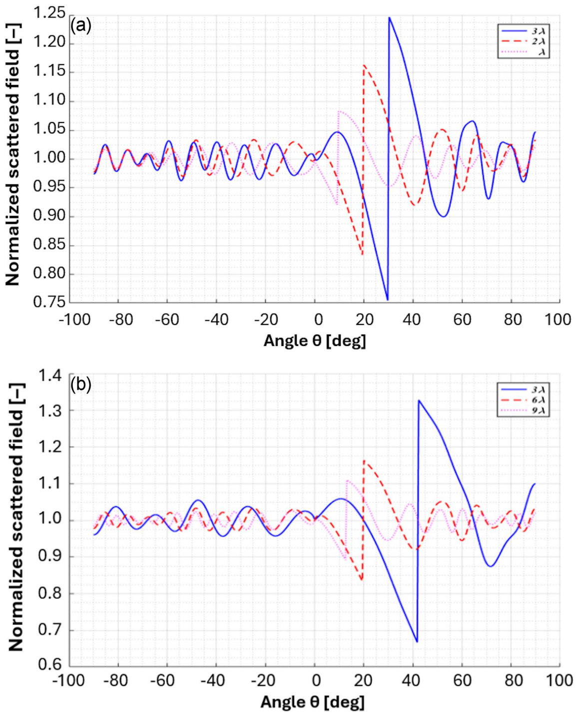

Fig. 4. Angular variation of the normalized scattered field for a circular PEC aperture: (a) effect of aperture radius a at $r = 6\lambda$, and (b) effect of observation distance r at $a = 2\lambda$. The wavelength is $\lambda = 0.1$ m, and the fields are normalized to the peak total-field magnitude at $\theta = 0^\circ$.

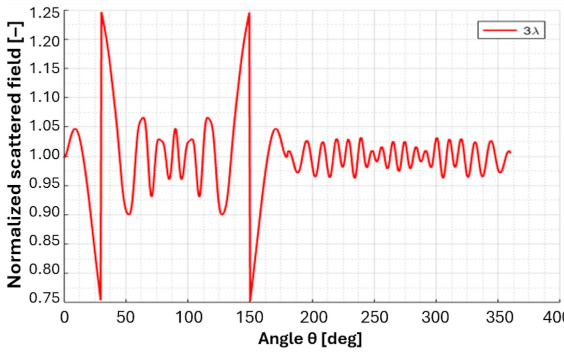

Fig. 5. Global angular profile of the normalized scattered field as a function of angle θ for a circular PEC aperture with $a = 3\lambda$. The observation angle is swept over $0^{\leq}\theta \leq 360^\circ$, and the field is normalized to the peak total-field magnitude at $\theta = 0^\circ$.

edge-integral representation. Known PEC aperture studies and full-wave benchmark solvers are therefore treated as reference validation routes for future work, whereas the present contribution focuses on a uniform analytical BDW-based representation and qualitative comparison of PEC-related angular field behavior [13, 14, 27]. Related wave-physics studies published in *Acta Physica Polonica A* have addressed edge diffraction, near-field optical interference, and electromagnetic-wave transmission in structured media, further demonstrating the continuing relevance of analytical and semi-analytical wave models in physics-oriented diffraction and propagation problems [30, 31].

Figure 4a and b illustrates the angular variation of the normalized scattered field obtained from the proposed detour-enhanced extended BDW formulation for a circular PEC aperture. In these simulations, the incident-field amplitude u_i was set to unity and the wavelength fixed at $\lambda = 0.1$ m. In Fig. 4a, the observation distance was held constant ($r = 6\lambda$), while the aperture radius was varied ($a = \lambda$, 2λ, 3λ). In Fig. 4b, the aperture radius was fixed ($a = 2\lambda$), and the observation distance was changed ($r = 3\lambda$, 6λ, 9λ). This two-parameter analysis enables simultaneous evaluation of geometric (a) and propagation (r) effects on the diffracted-field distribution.

Each curve in Fig. 4 represents the normalized magnitude of the diffracted field as a function of the observation angle θ. The horizontal axis corresponds to the observation direction relative to the aperture normal, whereas the vertical axis indicates the relative field amplitude normalized to its on-axis maximum. This representation visualizes the angular smoothness and spatial continuity of the field predicted by the analytical model. Consequently, these results provides both (i) an illustration of the continuous behavior of the formulation across the light–shadow boundary and (ii) a qualitative reference for engineering applications such as aperture and antenna design, where control of edge-diffraction characteristics is essential [18].

A pronounced feature visible in both panels of Fig. 4 is the well-defined, symmetric transition region near the shadow boundary. As the aperture radius a decreases (Fig. 4a), the transition zone narrows and the diffracted-field amplitude weakens, approaching the sub-wavelength-aperture limit. Increasing a enhances the transition behavior and reveals edge-enhanced oscillatory variations associated with the PEC rim. These oscillatory variations are interpreted as model-predicted edge-enhanced interference features produced by the incident, reflected, and diffracted contributions included in the proposed formulation, rather than as independently proven resonant modes [3, 18].

In Fig. 4b, increasing the observation distance r leads to a gradual attenuation of the diffracted field and a broadening of the angular response. The transition region persists but becomes less pronounced as the observation point moves away from the aperture, consistent with physical expectations in the far-field regime. Importantly, the field remains continuous and physically meaningful for all parameter combinations, a clear improvement over non-uniform boundary diffraction wave approaches that exhibit discontinuities near the shadow boundary [3, 4].

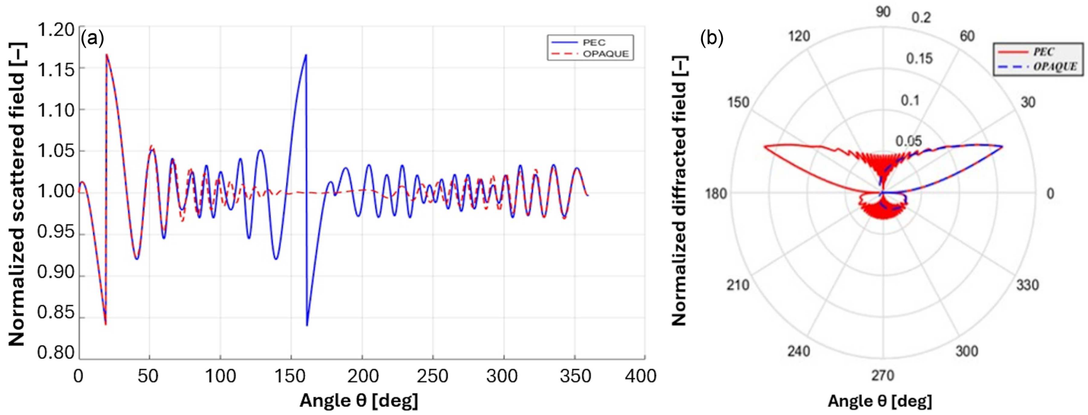

Fig. 6. Comparison of normalized scattered fields from circular apertures in PEC and opaque screens for $r = 6\lambda$, $a = 2\lambda$, and $\lambda = 0.1$ m: (a) Cartesian angular profile, and (b) polar angular distribution. All fields are normalized to the peak total-field magnitude at $\theta = 0°$.

Figure 5 presents the full 360° angular distribution of the normalized scattered field for a circular PEC aperture of radius $a = 3\lambda$. The observation angle θ was scanned continuously over region $0° \leq \theta \leq 360°$ to investigate field continuity, transition behavior, and global symmetry. This configuration allows direct inspection of the global field continuity and angular symmetry predicted by the analytical model. Each point in the figure represents the normalized field magnitude as a function of the observation angle. The horizontal axis corresponds to the observation direction relative to the aperture normal, while the vertical axis shows the field amplitude normalized to the on-axis maximum. This representation provides a direct visualization of the global uniformity of the analytical model, emphasizing the absence of unphysical jumps or discontinuities across all angular regions.

A key feature visible in Fig. 5 is the existence of two sharply defined transition regions, which correspond to the geometrical shadow boundaries. In contrast to classical BDW or opaque-aperture models, where amplitude discontinuities or numerical artifacts typically appear near these boundaries [3, 4, 18], the proposed detour-enhanced extended BDW framework produces a completely smooth field profile. The field passes continuously through both shadow edges, supporting the intended uniform behavior of the analytical formulation.

Another noteworthy aspect is the pronounced angular symmetry, where field maxima occur near the aperture-edge directions. The resulting lobes are interpreted as edge-enhanced field features associated with the PEC boundary and interference between reflected and diffracted contributions. Their reproduction supports the internal consistency of the proposed analytical formulation, while the present results should be understood as numerical evaluations of the derived expressions rather than independent full-wave validation. From a practical standpoint, obtaining smooth angular field profiles across the 360° domain is useful for high-frequency electromagnetic applications, including aperture analysis, antenna modeling, and scattering-control studies [18]. Figure 5 thus illustrates the global angular continuity and symmetry predicted by the proposed detour-enhanced extended BDW formulation.

Figure 6a and b presents a direct quantitative comparison of the scattered-field distributions produced by a circular aperture in a perfectly electrically conducting (PEC) surface and in an opaque (impenetrable) screen, evaluated for identical parameters ($r = 6\lambda$, $a = 2\lambda$, $\lambda = 0.1$ m). The results are shown in both Cartesian and polar representations to provide a comprehensive view of angular variation and radiation symmetry. Each curve in Fig. 6 represents the normalized scattered-field magnitude as a function of observation angle θ. The PEC result (solid line) exhibits pronounced oscillatory behavior and strong symmetry across the angular domain. This behavior arises from the reflective and conductive nature of the PEC boundary, which allows the incident field to be effectively reflected and re-radiated by the aperture. Consequently, edge-enhanced oscillatory lobes and angularly symmetric field patterns appear as PEC-related signatures within the present analytical formulation.

In contrast, the opaque aperture (dashed line) produces a considerably weaker and asymmetric field, especially in the source (shadow) region. Because classical BDW theory for opaque screens does not include any reflected component, its field is purely diffracted and cannot reproduce the reflection-induced continuity seen in the PEC case. As a result, the amplitude decreases sharply in the shadow region, and the oscillatory pattern largely vanishes, as clearly seen in the polar plot (Fig. 6b). These findings provide a comparative analytical visualization of the fundamental differences between PEC and opaque aperture models in the adopted BDW-based framework. The PEC aperture sustains a more symmetric and continuous angular field behavior because the reflected contribution is explicitly included in the formulation. The detour-enhanced extended BDW representation captures these reflection-driven features and maintains smooth transitions across the shadow boundaries, where classical non-uniform BDW models may exhibit discontinuities [3, 4, 18].

The agreement between the analytical predictions and the expected qualitative behavior of PEC aperture diffraction supports the internal consistency of the proposed formulation. The edge-enhanced field lobes and smooth angular evolution also emphasize the limitations of opaque-screen models when PEC reflection effects are relevant. Nevertheless, these results are not a substitute for independent full-wave validation by MoM, FEM, or FDTD solvers; rather, they demonstrate the continuity and computational compactness of the proposed detour-enhanced BDW representation.

The present formulation provides a unified analytical–numerical framework, bridging classical boundary-diffraction theory and modern electromagnetic design. Unlike existing BDW-based approaches, which are restricted to opaque geometries or paraxial conditions, the proposed detour-enhanced extended BDW theory offers a physically rigorous and computationally efficient way to model PEC apertures over the entire angular spectrum. This capability directly benefits high-frequency engineering problems where conventional numerical solvers are either unstable or computationally expensive — such as aperture antennas, radar scattering prediction, and metasurface optimization. By providing a mathematically continuous and computationally compact field representation, the method extends the applicability of BDW theory toward conductive aperture configurations and offers a useful analytical basis for future comparison with full-wave numerical solvers.

5. Conclusions

In this work, a uniform analytical formulation for electromagnetic scattering by a circular aperture in a perfectly electrically conducting (PEC) plane is developed in the framework of detour-enhanced extended boundary diffraction wave (BDW) theory. The formulation addresses the non-uniformity and discontinuity issues that arise in classical BDW descriptions near shadow boundaries by incorporating a detour-based phase correction and Fresnel-type uniformization. The resulting expressions provide a compact and continuous field representation over the considered angular range. Numerical evaluations based on the derived formulas illustrate smooth angular behavior, symmetric PEC-related field patterns, and edge-enhanced oscillatory features. In fact, these features are interpreted as interference-related effects of the PEC boundary rather than as independently proven resonant phenomena.

From a scientific standpoint, the presented formulation constitutes a major conceptual extension of the BDW theory, bridging the gap between geometrical and wave-based diffraction models. The method provides a rigorous analytical–numerical framework that transforms the classical scalar diffraction formulation into a generalized vector-consistent representation suitable for conductive boundaries. Its inherent uniformity ensures that the total field remains continuous, stable, and physically interpretable across illuminated, transition, and shadow regions, within the considered analytical framework, thereby providing a useful analytical reference for conductive aperture diffraction.

Beyond its theoretical significance, the proposed solution has direct engineering applicability. The ability to predict continuous, artifact-free scattered fields with high numerical efficiency makes it particularly valuable for modern electromagnetic design tasks, such as high-resolution radar cross-section prediction, aperture-antenna synthesis, beam-shaping systems, and reconfigurable metasurface architectures. The detour-enhanced BDW framework thus serves not merely as a theoretical construct but as a computationally efficient modeling tool that aligns with the accuracy requirements of next-generation high-frequency systems.

In conclusion, this study extends the analytical use of BDW theory by incorporating PEC-related reflected contributions into a detour-enhanced uniform edge-integral formulation for circular apertures. The resulting framework provides a compact analytical representation of conductive aperture diffraction and offers a scalable basis for future hybrid analytical–numerical comparisons. Future developments will target impedance and mixed-boundary configurations, broadband and time-domain extensions, and systematic validation against full-wave numerical solvers and experimental benchmarks.

References

[1] M. Born, E. Wolf, *Principles of Optics: Electromagnetic Theory of Propagation, Interference and Diffraction of Light*, Cambridge Univ. Press, Cambridge 1999.

[2] J.B. Keller, *J. Opt. Soc. Am.* **52**, 116 (1962).

[3] K. Miyamoto, E. Wolf, *J. Opt. Soc. Am.* **52**, 615 (1962).

[4] R. Borghi, *J. Opt. Soc. Am. A* **32**, 685 (2015).

[5] Y.Z. Umul, *J. Opt. Soc. Am. A* **27**, 1613 (2010).

[6] S. Ganci, *Optik* **119**, 41 (2008).

[7] J. Glückstad, A.E.G. Madsen, *Optik* **285**, 170950 (2023).

[8] C.J.R. Sheppard, *Photonics* **11**, 346 (2024).

[9] G. Apaydın, L. Sevgi, *Electromagnetic Diffraction Modeling and Simulation with MATLAB*, Artech House, Norwood (MA) 2021.

[10] H.R. Zeng, T. He, G. Fang, K. Li, *IEEE Trans. Antennas Propag.* **69**, 1345 (2021).

[11] H.D. Basdemir, *J. Opt. Soc. Am. A* **41**, 700 (2024).

[12] M. Lucido, G. Chirico, M.D. Migliore, D. Pinchera, F. Schettino, *Appl. Sci.* **13**, 7465 (2023).

[13] G. Lovat, P. Burghignoli, R. Araneo, S. Celozzi, *IET Microw. Antennas Propag.* **15**, 1147 (2021).

[14] V.M. Serdyuk, *Prog. Electromagn. Res. B* **102**, 99 (2023).

[15] Z. Wang, F. Kapsalidis, R. Wang, M. Beck, J. Faist, *Nat. Commun.* **13**, 230 (2022).

[16] F. Zhou, Y. Wu, Z. Zhang, X. Bai, C. Jiao, *IEEE Access* **10**, 116635 (2022).

[17] U. Yalçın, *Prog. Electromagn. Res. M* **7**, 29 (2009).

[18] M. Altınel, U. Yalçın, *Uludağ Univ. J. Fac. Eng.* **26**, 433 (2021).

[19] M. Altınel, U. Yalçın, *COMPEL* **43**, 269 (2024).

[20] K. Karaçuha, V. Tabatadze, E.I. Veliyev, *Int. J. Appl. Electromagn. Mech.* **68**, 13 (2022).

[21] A.S. Batoroev, *Opt. Express* **29**, 30419 (2021).

[22] A.H. Barnett, *J. Astron. Telesc. Instrum. Syst.* **7**, 021211 (2021).

[23] Y.-M. Gao, C.-J. Zu, X.-S. Xie, X.-Y. Yu, *Phys. Rev. A* **103**, 033519 (2021).

[24] C. Aime, S. Prunet, C. Theys, A. Ferrari, H. Lantéri, *Astron. Astrophys.* **686**, A240 (2024).

[25] R.G. Kouyoumjian, P.H. Pathak, *Proc. IEEE* **62**, 1448 (1974).

[26] H.A. Bethe, *Phys. Rev.* **66**, 163 (1944).

[27] A. Roberts, *J. Opt. Soc. Am. A* **4**, 1970 (1987).

[28] R.F. Harrington, *Proc. IEEE* **55**, 136 (1967).

[29] K.S. Yee, *IEEE Trans. Antennas Propag.* **14**, 302 (1966).

[30] J. Piechowicz, *Acta Phys. Pol. A* **119**, 1040 (2011).

[31] M. Kvapil, T. Šikola, V. Křápek, *Acta Phys. Pol. A* **142**, 668 (2022).